Optical Funneling and Trapping of Gold Colloids in Convergent Laser Beams

Andreas Königer and Werner Köhler*

Physikalisches Institut, Universität Bayreuth, D-95440 Bayreuth, Germany

ABSTRACT

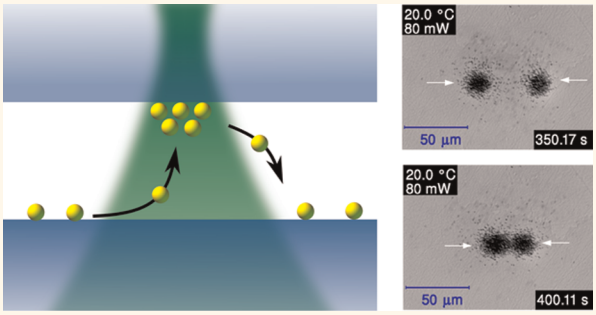

The simultaneous trapping of a large number of sedimenting Au colloids by optical radiation forces has been studied in detail. The particles are collected by a convergent laser beam and compressed against gravity and osmotic pressure at the upper window of the cell, thereby forming a dense colloidal gas. A minimum critical laser power is required to transport colloids into the trap. In contrast to conventional optical tweezers, the trap cannot be described by a 3D potential. Once the trap is sufficiently filled, the laser power can be reduced below the critical value, thereby stabilizing the trap population. Some characteristic properties of the trap, like the critical laser power and the transit time, are readily understood from a simple deterministic model. A detailed description that is capable of quantitatively accounting for the time dependence of the trap population, the finite leak rate at low power levels, or hysteresis effects requires the incorporation of fluctuations by means of a proper Langevin equation. Multiple independent traps are realized by time multiplexing of the laser beam, which allows for splitting up, independent manipulation, and subsequent recombination of a trapped colloidal cloud.

KEYWORDS: gold colloids · optical trapping · diffusion

Gold colloids attract researchers for a number of reasons. They differ from most other colloidal systems by their large density and optical absorption cross section. Their surface can be functionalized[1] and tailored for selective protein binding[2] or aggregate formation, for example.[3] Their large absorption cross section, due to the presence of the plasmon resonance,[4] allows for efficient heating by laser irradiation,[5−7] which can be utilized for cancer therapy.[8] Due to their small size, laser-heated gold colloids can be viewed as almost point-like heat sources that allow for localized heat release on length scales well below the optical diffraction limit. Heat release into the surrounding solvent has been shown to reduce the effective viscosity and increase the diffusion coefficient of the colloids.[5] When embedded in polymer solutions, the temperature field around laser-heated gold colloids couples to the polymer concentration *via* the Soret effect and leads to the formation of a cage of low viscosity around the particle due to depletion of the polymer.[9] Potentially, anomalous diffusion can be expected in such modulated viscosity landscapes.[10] Gold colloids embedded in microgel particles can modify their diffusion and thermodiffusion properties upon laser irradiation.[11] A number of authors have shown that not only dielectric particles[12] but also gold colloids can successfully be trapped and manipulated by optical radiation forces.[13−20] Recently, serial and parallel patterning of gold colloids by focused laser beams[21] and by holographic optical traps[22] has been demonstrated. Strong irradiation with excessive heating can lead to irreversible aggregation,[14,18] and even nonmetallic aggregates have been assembled by mere radiation pressure.[23] Svedberg *et al.* have accumulated silver nanoparticles in optical traps for surface-enhanced Raman scattering.[24−26]

In the present work, we show how sedimented gold colloids can be lifted up and collected in an almost two-dimensional cage by radiation forces that act against gravity and the osmotic pressure of the compressed colloidal gas. Once collected, the cloud of colloids can be manipulated in a number of ways. It can freely be moved to arbitrary positions, where, for example, specific chemical reaction could take place. By time-multiplexing of the laser beam, it is even possible to split the cloud into

* Address correspondence to werner.koehler@uni-bayreuth.de.

Received for review March 12, 2012 and accepted April 24, 2012.

Published online April 24, 2012
10.1021/nn301080a

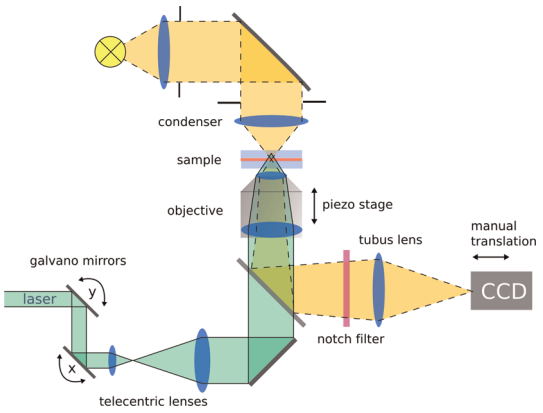

Figure 1. Inverted microscope setup with CCD camera, laser and galvano mirrors.

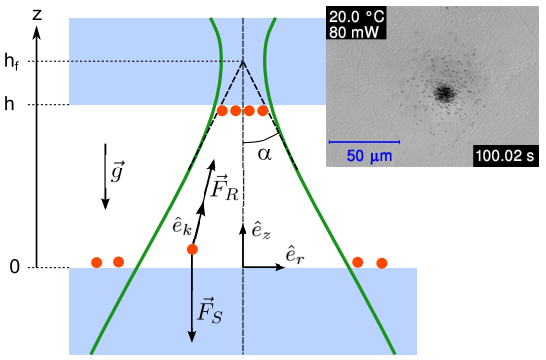

Figure 2. Left: sketch of the laser path through the sample cell. Right: accumulated Au colloids at the upper (exit) window.

sub-ensembles, which can then be manipulated independently and later be recombined by contact-free purely optical means.

All experiments described in this article were performed using an inverted microscope setup with bright-field illumination as shown in Figure 1. The laser beam (532 nm) is coupled into the microscope objective *via* a telecentric lens system. Horizontal displacement of the laser focus is accomplished by means of two galvano mirrors. The microscope is equipped with a piezo stage to focus the objective and define the vertical position of the laser focus within the sample. The plane of observation can be set independently from the focal plane with the laser focus by variation of the distance between the CCD camera and the tubus lens. The temperature was $T = 20$ °C.

RESULTS AND DISCUSSION

The basic principle of the experiment is illustrated in Figure 2 (left). The dispersed colloids ($R = 125$ nm) are contained within an optical cell (Hellma, 136-0.2-40-QS) with a quartz window of 1.2 mm thickness at the bottom and a height of the liquid layer of $h = 200$ μm. For improved thermal conductivity, the detachable upper quartz window has been replaced by a sapphire window of 1.0 mm thickness. The windows are aligned horizontally, perpendicular to the direction of gravity.

The laser beam, which enters the cell from below, is convergent within the sample volume. Its focal point is above the sample at $z = h_f$. With a microscope objective of effective NA = 0.33, the beam diameter at the lower (entrance) window at $z = 0$ is 124 μm. The diameter at the upper (exit) window at $z = 200$ μm can be adjusted over a broad range by shifting the vertical position of the focus, thereby changing the diameter at the entrance window only by a small fraction. In Figure 2, the upper diameter was set to 20.6 μm, corresponding to $h_f = 240$ μm, and the image plane was at the upper fluid sapphire interface at $z = 200$ μm.

If the laser power is sufficiently high, colloids within the light cone are lifted upward, pushed toward the upper window, and compressed toward the optical axis by the radiation forces, thereby substantially increasing the particle concentration (Figure 2 right). Despite their high number density, the particles remain in a gas-like state with rapid motion and repulsive interaction.

Deterministic Model. After the laser is turned on, a certain time is needed until the colloids reach the upper window and accumulate in the trap. The fastest particles are the ones that travel along the optical axis. Their appearance in the image plane defines the transit time. For a first approximation and in the case of relatively large colloids, as discussed here, diffusion can be neglected and the particles are treated like macroscopic objects.

The forces acting on a colloid (Figure 2) are gravity $\vec{F}_G$, buoyancy $\vec{F}_B$, and the radiation force $\vec{F}_R$. For a particle of radius R and density ρ_{Au}, the effective sedimentation force (gravity reduced by buoyancy) is

$$\vec{F}_S \equiv \vec{F}_G + \vec{F}_B = \frac{4}{3}\pi R^3(\rho_{Au} - \rho_{H_2O})\vec{g} \qquad (1)$$

wehre ρ_{Au} and ρ_{H_2O} are the densities of gold and water, respectively, and $\vec{g}$ is the gravitational acceleration.

The radiation force F_R contains contributions from both scattering and absorption.[27] Since the laser intensity is only moderate and the focus is outside of the sample volume, gradient forces, which are important for 3D trapping of single particles,[19] can be neglected. For Au colloids of $R \approx 125$ nm radius and the wavelength employed here of 532 nm, both the absorption cross section σ_{abs} and the scattering cross section σ_{sc} are approximately equal and identical to the geometric cross section:[4]

$$\sigma_{abs} \approx \sigma_{sc} \approx R^2\pi \qquad (2)$$

Assuming, for simplicity, isotropic scattering, the radiation force experienced by a colloid in a laser field of intensity I (in W/m^2) is

$$\vec{F}_R = \frac{\sigma_{abs} + \sigma_{sc}}{c} I\hat{e}_k = 2IR^2\pi\frac{n}{c_0}\hat{e}_k \qquad (3)$$

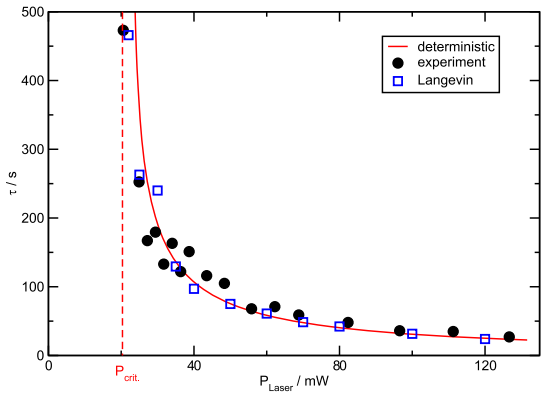

Figure 3. Transit time of the fastest colloid for various laser powers. The solid line shows an analytic solution of eq 9. The dashed line marks the critical laser power, where the deterministic radiation force at the lower entrance window compensates gravity. Also shown are results from simulations based on the Langevin equation (eq 13).

where c_0 is the speed of light in vacuum, n the refractive index of the medium (H_2O), and $\hat{e}_k$ a unit vector in the direction of the Poynting vector:

$$\hat{e}_k = -\sin\left(\arctan\frac{r}{h_f - z}\right)\hat{e}_r + \cos\left(\arctan\frac{r}{h_f - z}\right)\hat{e}_z \quad (4)$$

where r is the radial coordinate and $\hat{e}_z$ and $\hat{e}_r$ are unit vectors in z- and r-direction, respectively (Figure 2). The local laser intensity in the convergent Gaussian beam of total power P is

$$I(r,z) = \frac{2P}{\pi w^2(z)}\exp\left(-\frac{2r^2}{w^2(z)}\right) \quad (5)$$

with a z-dependent beam waist

$$w(z) = (h_f - z)\tan\alpha \quad (6)$$

The cone angle α is determined by the effective numerical aperture NA = n sin α = 0.33 of the microscope objective. Without laser irradiation, the colloids sediment close to the lower window with a characteristic layer thickness l_c determined from the barometric formula to $l_c = k_BT/F_S$ = 2.8 μm, thereby neglecting interparticle interactions.

As long as the laser intensity is weak, the colloids stay close to the lower wall. At a certain critical laser intensity I_c, first reached on the optical axis of the Gaussian beam profile, the upward pointing radiation force balances the downward pointing sedimentation force and the colloids are lifted from the lower window. Once started, the process is self-amplifying. After the particles have gained some height, the intensity of the convergent beam increases and the colloids accelerate.

Their drift velocity $\vec{v}_d(z,r)$ depends on the height z and the distance r from the optical axis. In a medium (water) of viscosity η, it is obtained by balancing the net force by the Stokes friction $-6\pi\eta R\vec{v}_d$:

$$\vec{v}_d(z,r) = \frac{\vec{F}_G + \vec{F}_B + \vec{F}_R(z,r)}{6\pi\eta R} \quad (7)$$

In the center of the beam, at $r = 0$, the sedimentation and radiation forces are antiparallel and the particle velocity becomes

$$v_d(z, r = 0) = \frac{1}{3\eta}\left[I(z, r = 0)R\frac{n}{c_0} - \frac{2}{3}R^2(\rho_{Au} - \rho_{H_2O})\right] \quad (8)$$

The minimum time needed for a particle to travel along the optical axis from the lower to the upper window is the transit time

$$\tau_t = \frac{h}{\langle v_d\rangle_t} \quad (9)$$

where the mean drift velocity is given by

$$\langle v_d\rangle_t = \left[\frac{1}{h}\int_0^h \frac{dz}{v_d(z,0)}\right]^{-1} \quad (10)$$

Figure 3 shows the measured transit time τ_t, taken at the appearance of the first colloid in the image plane at the upper window, as a function of laser power. The solid line is calculated according to eqs 3−10 without an adjustable parameter. The transit time diverges at the critical laser power P_{crit} = 20.3 mW, below which the radiation forces are too weak to overcome gravity. The good agreement between analytical model and experiment is an indication that no essential ingredients have been omitted and other possible transport processes like convection or thermodiffusion are not relevant for the fastest particles.

Also shown in Figure 3 are simulation results based on the Langevin equation discussed below. There is a good agreement between experiment, stochastic simulation, and deterministic model—in particular for high laser powers. The deviations become noticeable only near the critical laser power, where the deterministic model significantly overestimates the measured and simulated transit times. This is a first hint that fluctuations may become decisive at low laser intensities.

One-Dimensional and Two-Dimensional Potentials. In contrast to conventional optical trapping near the focus of a sharply focused laser beam,[28,29] where nonconservative forces yield negligible effects,[30] it is not possible to define a 3D potential for our trap since $\nabla \times \vec{F}_R \neq 0$. As a consequence, the spatial colloid density cannot be obtained from a Boltzmann distribution. Potentials exist, however, for the special cases of restricted 1D motion along and for 2D motion perpendicular to the optical axis.

The axial 1D potential is given by

$$U_1(z) = \int_0^z [\vec{F}_G + \vec{F}_B + \vec{F}_R(z', r = 0)]dz' \quad (11)$$

It is plotted in Figure 4 for different laser powers.

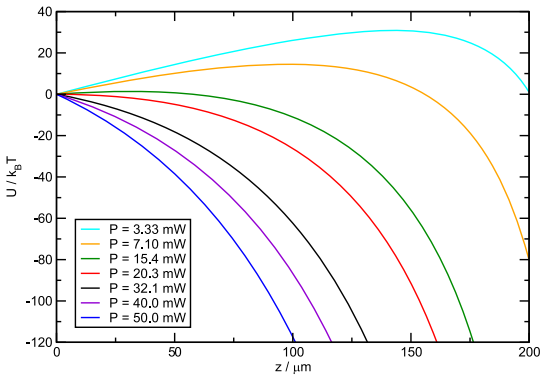

Figure 4. Calculated trap potential for 1D motion along the optical *z*-axis at *r* = 0.

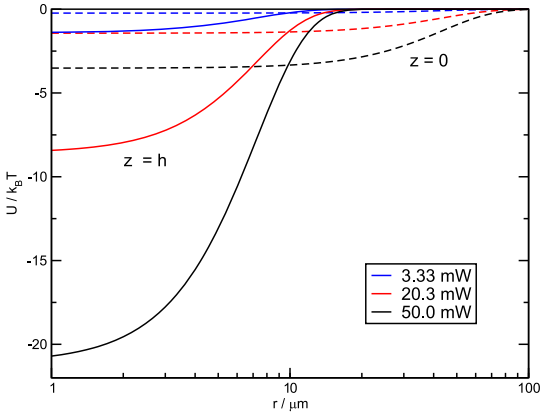

Figure 5. Calculated radial trap potential for 2D motion perpendicular to the optical axis along the surface of the upper (*z* = *h*, solid lines) and lower (*z* = 0, dashed lines) window for three different laser powers given in the legends.

Even for the critical laser power P_{crit} = 20.3 mW, where the potential starts with zero slope at the lower window at $z = 0$, the depth of the well at $z = h$ exceeds 100 k_BT, making it impossible for the particles to escape from the trap along this trajectory. For the lowest laser power of 3.3 mW, the potential energies of the colloids at the lower and upper window are identical but the barrier that efficiently separates these two states along the *z*-axis still amounts to 30 k_BT with a position of the maximum at $z \approx 142$ μm.

The 2D potential for lateral motion perpendicular to the optical axis is

$$U_2(r,z) = -\int_r^\infty I(r',z)\sin\left(\arctan\frac{r'}{h_f - z}\right)dr' \quad (12)$$

It is of particular importance at the lower ($z = 0$) and upper ($z = h$) window. These two cases are plotted in Figure 5.

For high laser power, the depth of the radial potential well at the upper window is many k_BT and the radial excursion of the colloids, which are pushed against the window by the axial component of the radiation force, is limited to a few micrometers. In the case of lower laser power, in particular, for the axially bistable state (3.3 mW), the potential is only on the order of k_BT and too shallow for an efficient lateral confinement.

At the lower window, where the beam is still significantly expanded, the radiation forces are reduced by a factor of $(w(0)/w(h))^2 = (124\ \mu m/20.6\ \mu m)^2 \approx 36$, corresponding to a reduction of the depth of the potential well by a factor of $w(0)/w(h) \approx 6$. In particular, above P_{crit} = 20.3 mW, the depth is sufficient to cause a net diffusion flux from the periphery toward the center, where the lift force transports the particles toward the trap at the upper window.

Stochastic Forces. Although the above deterministic description gives a good estimation of, for example, the transit time and the critical laser power, details of the optical trap can only be understood when the stochastic forces acting on the colloid are also taken into account. In particular, the transport of colloids that start at a certain lateral distance from the optical axis, where the laser power at the lower window is insufficient for lift-off, and the finite leak rate of the trap at low laser powers cannot be described without proper incorporation of diffusion.

Single particle diffusion under the influence of thermal agitation is described by adding a random fluctuating force $\vec{\xi}(t)$ to eq 7 to obtain the Langevin equation

$$6\pi\eta R\vec{v}_d(z,r) = \vec{F}_G + \vec{F}_B + \vec{F}_R(z,r) + \vec{\xi}(t) \quad (13)$$

Inertia terms can safely be neglected on time scales $t > m(6\pi\eta R)^{-1} \approx 70$ ns. The isotropic fluctuating force represents white noise with an amplitude defined by the fluctuation–dissipation theorem:[5]

$$\langle\vec{\xi}(t)\rangle = 0 \quad (14)$$

$$\langle\xi_i(t)\xi_j(t')\rangle = 12k_BT\pi\eta R\delta(t - t')\delta_{ij} \quad (15)$$

A first direct consequence of thermal agitation is that sedimented particles starting at the lower boundary at a certain distance from the optical axis, where the vertical radiation force is still too low to overcome gravity, are not necessarily pushed toward the optical axis by the horizontal component of the radiation force. Due to their Brownian motion, there is now a certain chance for these colloids to escape the funnel of the trap. Two representative trajectories of particles starting at the same initial distance r_0 from the optical axis are shown in Figure 6 for illustration.

Of course, it is also possible that colloids diffuse from the periphery into the laser beam and eventually end up in the trap, which would not be observed in the purely deterministic case. The consequence is a net inward flow of particles into the trap that contains a diffusion term due to the developing radial

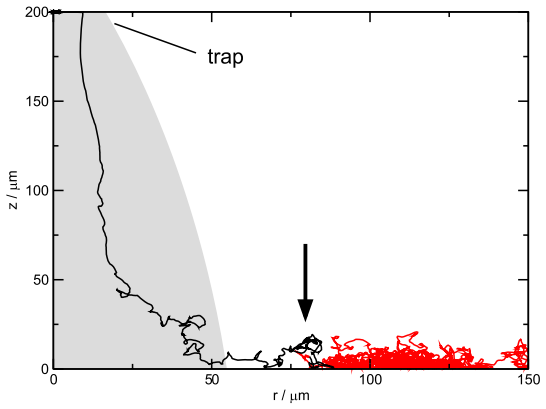

Figure 6. Simulated trajectories of two test particles starting at $z = 0$ and a distance $r_0 = 80\ \mu$m (arrow) from the optical axis. Laser power = 100 mW. Within the shaded area, the photonic lift force exceeds sedimentation.

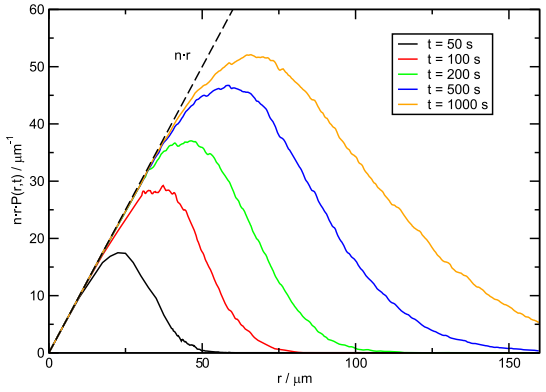

Figure 7. Distribution of the colloids within the trap as a function of their initial distance from the optical axis for selected times *t*. The curves have been obtained from up to 10^4 simulated trajectories. Laser power = 100 mW; n = 1 μm^{-2} is the initial sedimented colloid density, and $P(r,t)$ is the probability of finding a colloid with initial distance r from the axis at time t within the trap.

concentration gradient and a drift term due to the radial component of the radiation force.

The colloids starting close to the optical axis are the first to appear in the trap at the upper window. Since the number of particles that start at a certain distance r from the axis increases linearly with r but their chance to reach the trap within a given time t decreases, there exists a certain distance r_{max} from where most particles in the trap have originated. The r_{max} increases with time since all particles starting close to the axis are already within the trap and more particles from the periphery arrive. Figure 7 shows the distribution of the trapped particles as a function of their initial starting distance from the axis for a number of different times t. The total number corresponding to the area under the curves increases, and the maximum shifts toward larger radii. The dashed asymptote that is reached for small r corresponds to the situation where all colloids starting at this distance have already reached the trap.

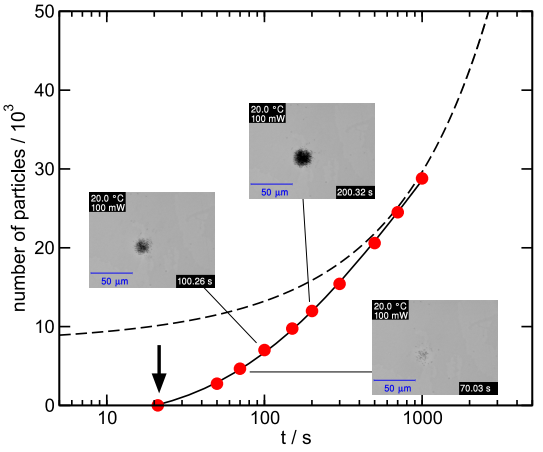

Figure 8. Number of particles within the trap as function of time obtained from integration of the distribution functions in Figure 7 (filled circles, solid line). Experimental micrographs at selected times for comparison. The arrow marks the transit time. Laser power P = 100 mW. Dashed line: solution of simplified diffusion model (eq 16).

The total number of trapped colloids at time t is obtained by integrating the distributions in Figure 7. This is plotted in Figure 8 together with selected images. While it is impossible to resolve and count the individual particles, the qualitative agreement between the model and the experiment is convincing. The only obvious deviation is that the trap initially (at 70 s) contains too few particles when compared to later times. This is most likely due to shadowing effects of the colloids at the lower window which somewhat reduce the effective laser power experienced by the fastest colloids.

The asymptotic filling of the trap is controlled by the colloids diffusing from the periphery into the laser beam. For long times, details of the upward transport from the lower window into the trap are not important and the problem can be modeled as diffusion on a disk with a hole in the center, where the particles dissappear as soon as they touch the inner rim (first passage problem). This is equivalent to the problem of radial diffusion in a hollow cylinder of infinite length. The inner radius r_a is defined by the diameter of the laser beam where the intensity is sufficient for lift-off, around $r = r_a \approx 50\ \mu$m in Figure 7, with the boundary condition of zero concentration: $c(r_a) = 0$. The outer radius r_b is on the order of the size of the cuvette, $r_b \approx$ 1000 μm, which is effectively infinite for all relevant times considered here. The outer boundary condition is $c(r_b) = c_0$, with c_0 being the mean initial colloid concentration. An analytic solution of the radial diffusion equation

$$\frac{\partial c}{\partial t} = \frac{1}{r}\frac{\partial}{\partial r}\left(rD\frac{\partial c}{\partial r}\right) \qquad (16)$$

for the given boundary conditions can be found in refs 31 and 32. Due to the very slow convergence of an

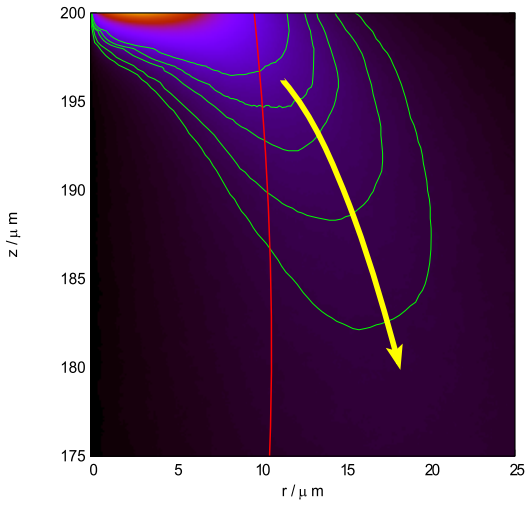

Figure 9. Escape of particles from the trap for a laser power of P = 3.3 mW. The color encodes the simulated particle density, which is high inside the trap at $z \approx 200$ μm and $r <$ 10 μm. The arrow indicates the main escape path. To the right of the almost vertical line at $r \approx 10$ μm, sedimentation exceeds the upward pointing radiation force.

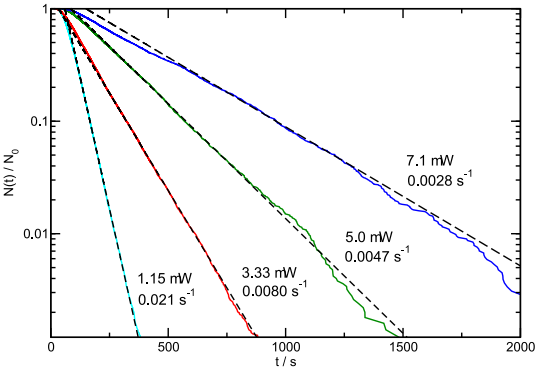

Figure 10. Simulated leakage of the trap for different laser powers. The leak rates (in s^{-1}) are obtained from the slopes at long times.

infinite alternating series of Bessel functions, it is, however, more convenient to solve the partial differential (eq 16) numerically. Using $D = k_BT/(6\pi\eta R) = 1.71 \times 10^{-12}$ m^2/s, the result of this simplified model is plotted in Figure 8 as the dotted line. The deviations at short times are due to details of the transport of the colloids into the trap volume after they have reached the laser beam. At longer times ($t >$ 500 s), these details become less important and the growth of the trap population asymptotically approaches the solution of eq 16.

Leakage of the Trap. When the laser power is lowered from high values to below P_{crit} = 20.3 mW, new particles can no longer efficiently be transported into the trap. Colloids that are already inside the trap can initially be kept there due to the still very deep potential along the z-axes (4) and the almost 10 k_BT deep radial potential (5). A further reduction, however, leads to an increasing particle loss from the trap. In Figure 9, this leakage has been analyzed by numerical

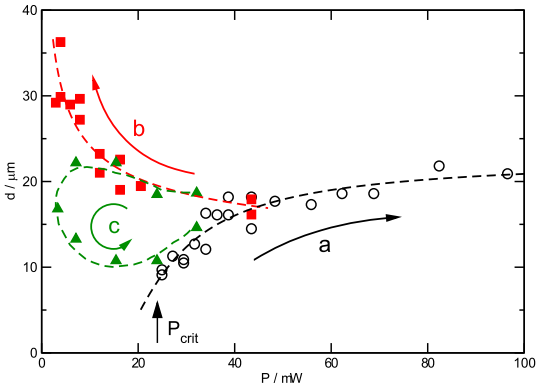

Figure 11. Diameter d of the trapped particle cloud as a function of laser power P for slow increase (a), rapid decrease (b), and slow cycle (c) of P. The dashed lines are guides to the eye and approximate the cloud diameter during the changes of the laser power indicated by the arrows.

integration of eq 13 for the very low laser power of 3.3 mW, which would, without diffusion, still be sufficient to constrain the particles. Interactions between the colloids have been neglected, corresponding to a situation where only few particles are inside the trap (single particle limit). The color-coded contour plot shows the particle density within the upper 25 μm of the cell, which has been obtained from a simulation of 10^4 particle trajectories over 500 s of laboratory time. To the left of the almost vertical curve near r = 10 μm, the radiation lift force exceeds sedimentation. To the right, gravity wins and the colloids sediment. Inside the trap, the colloids are still vertically confined near the upper window. The radial potential, however, is not sufficiently deep, only 0.23 k_BT, to prevent particles from leaving the trap and crossing into the sedimentation region. Some colloids can re-enter the trap by diffusing back into the left region with small r, where they are again transported upward, but the majority irreversibly escapes the trap and sediments. Note that the region with deterministic upward transport only extents down to $z \approx 140$ μm for P = 3.3 mW.

Figure 10 shows the decay of the trap population due to leakage for different relatively low laser powers. For practical purposes, a particle is considered to have escaped from the trap once it has reached a critical height below z_{crit} = 160 μm, from where the probability to return into the trap is almost negligible. For long times, the decays are nicely exponential, whereas for short times, there is some deviation due to the finite time needed to reach z_{crit}. For high laser powers above P_{crit}, the leak rate tends to zero for all practical purposes.

Particle Interaction and Hysteresis. If the number of colloids within the trap becomes large, interparticle interactions become increasingly important. A high concentration of repulsive particles leads to an increase of the osmotic pressure and, as a consequence,

to an increase of the diffusion coefficient, a swelling of the cloud of trapped colloids, and to an increase of the leak rate.

The diameter and the population of the particle cloud depend on the laser power and on the history of the experiment in a complicated manner. As a consequence, even hysteresis loops can be encountered when the trap is driven through a cycle with increasing and decreasing laser power. This is demonstrated in Figure 11, where the experiment has been conducted as follows:

Initially, the trap is empty and—starting from zero—the laser power is set to stepwise increasing values and kept there for a fixed period of 200 s after the first colloids appear in the trap (transit time). After crossing P_{crit}, the first colloids appear in the trap. Subsequently, the population of the trap grows because of both the longer waiting time (7) and the steadily increasing laser power. The diameter of the cloud, as plotted in Figure 11 (trace a), increases due to the increasing osmotic pressure, which overcomes the counteracting compression by the also increasing inward pointing radial radiation force.

The temperature field around the colloids leads to a decrease of the effective viscosity and, hence, to an increase of the diffusion coefficient D. This effect has been termed *hot Brownian motion* and has been discussed in detail in ref 5. Neglecting wall effects, we estimate the increase of D due to heating to approximately 7% for 20 mW laser power.

These two effects can be separated by first increasing the laser power along trace a, up to say 50 mW, followed by a rapid decrease (trace b). During this quench, the leakage of the trap can be neglected and the number of particles and, hence, the osmotic pressure remain constant, whereas the radiation pressure decreases. As a result, the diameter of the cloud approximately doubles. Note that a populated state below P_{crit} can only be reached *via* such a route since no new particles can enter the trap at these low laser powers. Due to the finite leak rates, the trap slowly loses particles in this parameter range. A rapid quench along trace b followed immediately by rapid power increase is essentially reversible along the same trajectory.

If the laser power is not changed rapidly but is slowly cycled down to some minimum value and then back up again, leakage of the trap at low power levels becomes important and the system is driven through a hysteresis loop (trace c). The cloud diameter at a certain laser power increases with the number of trapped particles, but no quantitative relation can be given since it is not possible to count the number of trapped colloids.

Manipulation of the Trapped Colloids. The trapped particles can be transferred to an arbitrary position by slowly moving the laser beam. In order to constrain the colloids within the moving trap, the Stokes friction caused by a motion of the trap with a velocity $\dot{\vec{r}}_0(t)$ must not exceed the radiation forces that laterally compress the colloidal cloud. If hydrodynamic interactions between the colloids are neglected, the effect is readily described by the Langevin eq 13 after introducing a time-dependent position of the center of the laser beam in eq 5 as $I(|\vec{r} - \vec{r}_0(t)|,z)$.

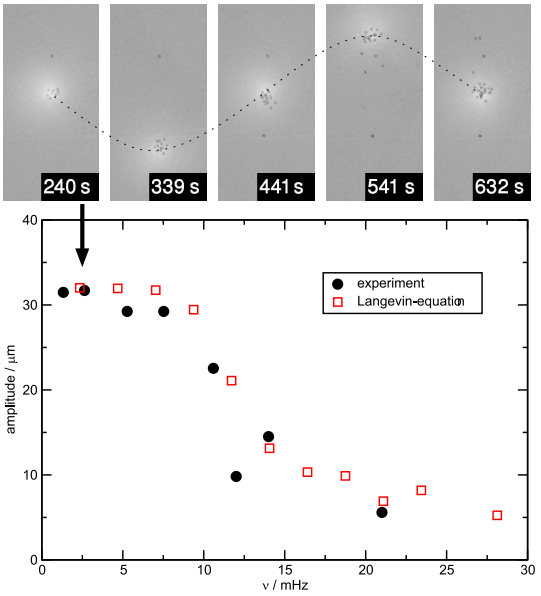

Figure 12. Displacement of the laser trap with a sinusoidal amplitude of 32 μm and a laser power of 50 mW. Top: displacement of the colloidal cloud during one period (ν = 2.6 mHz). The micrographs also show some colloids that are immobilized at the window surface. Bottom: amplitude of the colloid displacement as function of the trap displacement frequency ν.

Figure 12 shows experiments with a sinusoidal laser beam displacement with fixed amplitude (32 μm) and variable frequency ν, measured with a small number of colloids in the trap to minimize effects due to hydrodynamic coupling. For low frequencies, the cloud entirely follows the trap, but with increasing frequency, friction becomes too large and the displacement amplitude decreases. Also shown are data from a simulation based on eq 13, which match the experiment without any adjustable parameter.

Multiple traps can be implemented by rapidly switching the laser beam between different positions, which can be steered independently. By splitting an initial populated trap into two time multiplexed ones, which are then slowly moved apart, it is possible to divide the colloids into two independent clouds that can be directed to different positions and manipulated independently. Later, they can be recombined. Such an experiment is shown in Figure 13, where a trapped cloud of particles is split into two independent ones that are separated and then again brought together.

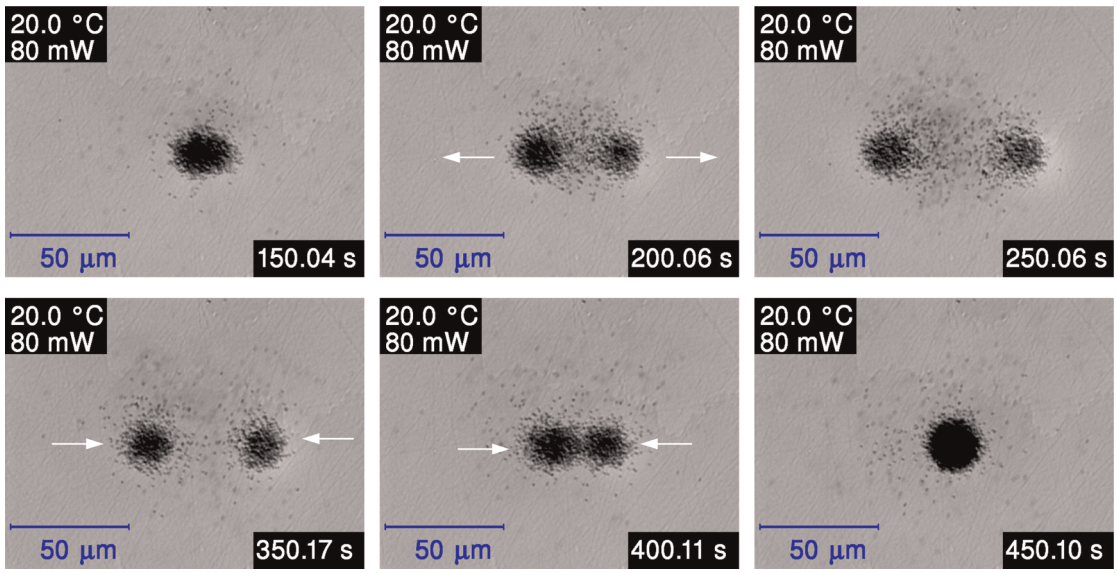

Figure 13. Splitting and recombining trapped colloid cloud by two time multiplexed and independently controlled traps.

TABLE 1. Numerical Values of Characteristic System Parameters at T = 20 °C (η, ρ_{Au}, and ρ_{H_2O} from ref 37)

quantity	symbol	value	unit
colloid radius	R	125	nm
viscosity	η	1.005×10^{-3}	Pa s
density Au	ρ_{Au}	19.3×10^{3}	kg/m^3
density H_2O	ρ_{H_2O}	0.998×10^{3}	kg/m^3

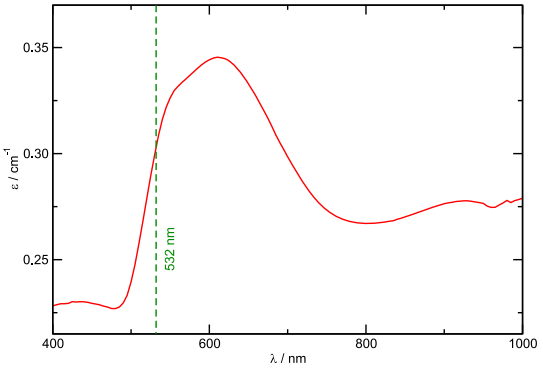

Figure 14. Measured extinction coefficient of the Au nanoparticle dispersion.

SUMMARY AND CONCLUSIONS

We have discussed in detail how relatively large gold colloids with a radius exceeding 100 nm can be accumulated and manipulated in an optical trap. Due to their size and high density, the colloids sediment very close to the bottom of the sample cell. By irradiation with a convergent laser beam into their plasmon absorption band, they are lifted up and accumulate at the upper cell window. At the same time, they are compressed toward the optical axis by the radial radiation forces in the light cone. A large number of colloids can be accumulated in the trap, but the confinement along the optical z-axis cannot be achieved by the inhomogeneous electric light field and requires the impermeable boundary of the upper cell window. Depending on the distance from the optical axis, a distribution of transfer times of the colloids into the trap is observed, and the fastest particles that travel along the optical axis define the transit time.

Although some properties of the trap, like the existence of a critical laser power and the transit time, are readily described by a purely deterministic picture, essential features can only be understood when thermal agitation is taken into account. The effect of stochastic noise is two-fold. On one side, it increases the trap population since particles can diffuse from the periphery into the laser beam. On the other side, diffusion is also responsible for a leakage of the trap at low laser power.

Because the critical threshold laser power for the transport of the colloids into the trap and the much lower laser power required to keep the particles there, the trap can be populated with an almost arbitrary number of colloids that are then confined on time scales below the characteristic trap lifetime. For our system, the lifetime of the trap, as defined by the inverse of the leak rate (10), exceeds 10^3 s for laser powers above 10 mW. Thus, there exists a window where rather stable trap populations can be sustained for long times a few millwatts below the critical laser power P_{crit} = 20.3 mW.

Time multiplexing of the laser position allows for the creation of multiple independent traps, which can be used to split a colloidal cloud into two, or even multiple, parts that can be manipulated independently and transferred to arbitrary locations. Possibly, this opens an interesting route toward selective chemistry of surface-functionalized gold colloids at different spatial positions with the option of subsequent recombination

of the sub-ensembles. Despite the significant temperature gradients around a heated colloid, no interaction between the particles that could be attributed to thermodiffusion[33] has been observed. The absence of a noticeable Soret effect is most likely due to the high thermal conductivity of gold, which short circuits the temperature gradient across the colloid. We also did not observe noticeable light-induced interaction between the gold colloids, as has been reported for metal nanoparticles[34] and for magnetic colloids.[35,36]

EXPERIMENTAL DETAILS

Instrumentation. An Olympus IX-71 inverted microscope with a 40× objective (Olympus LUCPlanFLN) was used in bright-field illumination. The laser (Coherent Verdi, 532 nm, TEM_{00}) was coupled into the back port *via* a telecentric lens system and two galvano mirrors (Cambridge Technology model 6220). The laser power was measured in front of the backport of the microscope and rescaled with an experimentally determined attenuation factor for the sample position. A piezo stage (Piezosystem Jena Mipos) was used for focusing. Images were acquired with a 12 bit CCD camera (PCO PixelFly QE) at a rate of approximately 3 Hz. The temperature was stabilized to $T = 20 \pm 0.1$ °C by means of a circulating water thermostat (Julabo CF31).

Material. The dispersed gold colloids were obtained from BBInternational (EM.GC250). They have a nominal radius of $R = 125$ nm and a number density of 3.6×10^8 mL^{-1} (Table 1). They are dispersed in water and electrostatically stabilized against aggregation.

The measured extinction coefficient (Figure 14) of the nanoparticle dispersion at the laser wavelength is $\varepsilon = 0.30$ cm^{-1}, which is in good agreement with the value of $\varepsilon = 0.35$ cm^{-1} calculated from the number density and the geometric cross section as described in the text (eq 2). Since the uncertainty of the colloid number density is not known and because of possible sedimentation problems of the sample during the measurement of the absorption spectrum, the calculated cross section has been used througout the article.

Conflict of Interest: The authors declare no competing financial interest.

Acknowledgment. We thank F. Busse, W. Zimmermann, A. Krekhov, and V. Weith for helpful discussions. This work has been supported by the Deutsche Forschungsgemeinschaft (Research Unit FOR608/TP6).

REFERENCES AND NOTES

1. Neouze, M.-A.; Schubert, U. Surface Modification and Functionalization of Metal and Metal Oxide Nanoparticles by Organic Ligands. *Monatsh. Chem.* **2008**, *139*, 183–195.
2. Kogan, M. J.; Bastus, N. G.; Amigo, R.; Grillo-Bosch, D.; Araya, E.; Turiel, A.; Labarta, A.; Giralt, E.; Puntes, V. F. Nanoparticle-Mediated Local and Remote Manipulation of Protein Aggregation. *Nano Lett.* **2006**, *6*, 110–115.
3. Hussain, I.; Wang, Z.; Cooper, A. I.; Brust, M. Formation of Spherical Nanostructures by the Controlled Aggregation of Gold Colloids. *Langmuir* **2006**, *22*, 2938–2941.
4. van Dijk, M. A.; Tchebotareva, A. L.; Orrit, M.; Lippitz, M.; Berciaud, S.; Lasne, D.; Cognet, L.; Lounis, B. Absorption and Scattering Microscopy of Single Metal Nanoparticles. *Phys. Chem. Chem. Phys.* **2006**, *8*, 3486–3495.
5. Rings, D.; Schachoff, R.; Selmke, M.; Cichos, F.; Kroy, K. Hot Brownian Motion. *Phys. Rev. Lett.* **2010**, *105*, 090604.
6. Govorov, A.; Richardson, H. H. Generating Heat with Metal Nanoparticles. *Nano Today* **2007**, *2*, 30–38.
7. Bendix, P. M.; Reihani, S. N. S.; Oddershede, L. B. Direct Measurements of Heating by Electromagnetically Trapped Gold Nanoparticles on Supported Lipid Bilayers. *ACS Nano* **2010**, *4*, 2256–2262.
8. Zhang, J. Z. Biomedical Applications of Shape-Controlled Plasmonic Nanostructures: A Case Study of Hollow Gold Nanospheres for Photothermal Ablation Therapy of Cancer. *J. Phys. Chem. Lett.* **2010**, *1*, 686–695.
9. Schwaiger, F.; Zimmermann, W.; Köhler, W. Transient Cage Formation around Hot Gold Colloids Dispersed in Polymer Solutions. *J. Chem. Phys.* **2011**, *135*, 224905.
10. Burgis, M.; Schaller, V.; Glässl, M.; Kaiser, B.; Köhler, W.; Krekhov, A.; Zimmermann, W. Anomalous Diffusion in Viscosity Landscapes. *New J. Phys.* **2011**, *13*, 043031.
11. Spill, R.; Köhler, W.; Lindenblatt, G.; Schaertl, W. Thermal Diffusion and Soret Feedback of Gold-Doped Polyorganosiloxane Nanospheres in Toluene. *Phys. Rev. E* **2000**, *62*, 8361–8368.
12. Ashkin, A.; Dziedzic, J. M. Optical Levitation by Radiation Pressure. *Appl. Phys. Lett.* **1971**, *19*, 283–285.
13. Svoboda, K.; Block, S. M. Optical Trapping of Metallic Rayleigh Particles. *Opt. Lett.* **1994**, *19*, 930–932.
14. Zhang, Y.; Gu, C.; Schwartzberg, A. M.; Chen, S.; Zhang, J. Z. Optical Trapping and Light-Induced Agglomeration of Gold Nanoparticle Aggregates. *Phys. Rev. B* **2006**, *73*, 165405.
15. Furukawa, H.; Yamaguchi, I. Optical Trapping of Metallic Particles by a Fixed Gaussian Beam. *Opt. Lett.* **1998**, *23*, 216–218.
16. Seol, Y.; Carpenter, A. E.; Perkins, T. T. Gold Nanoparticles: Enhanced Optical Trapping and Sensitivity Coupled with Significant Heating. *Opt. Lett.* **2006**, *31*, 2429–2431.
17. Yoshikawa, H.; Matsui, T.; Masuhara, H. Reversible Assembly of Gold Nanoparticles Confined in an Optical Microcage. *Phys. Rev. E* **2004**, *70*, 061406.
18. Sato, S.; Harada, Y.; Waseda, Y. Optical Trapping of Microscopic Metal Particles. *Opt. Lett.* **1994**, *19*, 1807–1809.
19. Hansen, P. M.; Bhatia, V. K.; Harrit, N.; Oddershede, L. Expanding the Optical Trapping Range of Gold Nanoparticles. *Nano Lett.* **2005**, *5*, 1937–1942.
20. Messina, E.; Cavallaro, E.; Cacciola, A.; Iati, M. A.; Gucciardi, P. G.; Borghese, F.; Denti, P.; Saija, R.; Compagnini, G.; Meneghetti, M.; *et al.* Plasmon-Enhanced Optical Trapping of Gold Nanoaggregates with Selected Optical Properties. *ACS Nano* **2011**, *5*, 905–913.
21. Guffey, M. J.; Scherer, N. F. All-Optical Patterning of Au Nanoparticles on Surfaces Using Optical Traps. *Nano Lett.* **2010**, *10*, 4302–4308.
22. Nedev, S.; Urban, A. S.; Lutich, A. A.; Feldmann, J. Optical Force Stamping Lithography. *Nano Lett.* **2011**, *11*, 5066–5070.
23. Hofkens, J.; Hotta, J.; Sasaki, K.; Masuhara, H.; Iwai, K. Molecular Assembling by the Radiation Pressure of a Focused Laser Beam: Poly(*N*-isopropylacrylamide) in Aqueous Solution. *Langmuir* **1997**, *13*, 414–419.
24. Svedberg, F.; Käll, M. On the Importance of Optical Forces in Surface-Enhanced Raman Scattering (SERS). *Faraday Discuss.* **2006**, *132*, 35–44.
25. Svedberg, F.; Li, Z.; Xu, H.; Käll, M. Creating Hot Nanoparticle Pairs for Surface-Enhanced Raman Spectroscopy through Optical Manipulation. *Nano Lett.* **2006**, *6*, 2639–2641.
26. Tong, L.; Righini, M.; Gonzalez, M. U.; Quidant, R.; Käll, M. Optical Aggregation of Metal Nanoparticles in a Microfluidic Channel for Surface-Enhanced Raman Scattering Analysis. *Lab Chip* **2009**, *9*, 193–195.
27. Saija, R.; Denti, P.; Borghese, F.; Marago, O. M.; Iati, M. A. Optical Trapping Calculations for Metal Nanoparticles. Comparison with Experimental Data for Au and Ag Spheres. *Opt. Express* **2009**, *17*, 10231–10241.
28. Sasaki, K.; Tsukima, M.; Masuhara, H. Three-Dimensional Potential Analysis of Radiation Pressure Exerted on a Single Microparticle. *Appl. Phys. Lett.* **1997**, *71*, 37–39.

29. Pralle, A.; Prummer, M.; Florin, E.-L.; Stelzer, E. H. K.; Hörber, J. K. H. Three-Dimensional High-Resolution Particle Tracking for Optical Tweezers by Forward Scattered Light. *Mircrosc. Res. Tech.* **1999**, *44*, 378–386.
30. Pesce, G.; Volpe, G.; Luca, A. C. D.; Rusciano, G.; Volpe, G. Quantitative Assessment of Non-conservative Radiation Forces in an Optical Trap. *Europhys. Lett.* **2009**, *85*, 38002.
31. Crank, J. *The Mathematics of Diffusion*; Clarendon Press: Oxford, 1970.
32. Carslaw, H. S.; Jaeger, J. C. *Conduction of Heat in Solids*; Clarendon Press: Oxford, 2001.
33. Di Leonardo, R.; Ianni, F.; Ruocco, G. Colloidal Attraction Induced by a Temperature Gradient. *Langmuir* **2009**, *25*, 4247–4250.
34. Zelenina, A. S.; Quidant, R.; Nieto-Vesperinas, M. Enhanced Optical Forces between Coupled Resonant Metal Nanoparticles. *Opt. Lett.* **2007**, *32*, 1156–1158.
35. Kellner, R. R.; Köhler, W. Short-Time Aggregation Dynamics of Reversible Light-Induced Cluster Formation in Ferrofluids. *J. Appl. Phys.* **2005**, *97*, 034910.
36. Hoffmann, B.; Köhler, W. Reversible Light-Induced Cluster Formation of Magnetic Colloids. *J. Magn. Magn. Mater.* **2003**, *262*, 289–293.
37. Mende, D.; Simon, G. *Physik, Gleichungen und Tabellen*; VEB Fachbuchverlag: Leipzig, 1976.